Published in final edited form as:
J Am Chem Soc. 2007 August 15; 129(32): 9852–9853. doi:10.1021/ja073506r.

Surface Modification and Functionalization of Nanoscale Metal-Organic Frameworks for Controlled Release and Luminescence Sensing

William J. Rieter, **Kathryn M. L. Taylor**, and **Wenbin Lin**
Department of Chemistry, University of North Carolina, Chapel Hill, NC 27599

Metal-organic frameworks (MOFs) are an interesting class of materials which have been exploited on the bulk scale for a number of applications, including gas adsorption[1] and catalysis.[2] We have recently described a general method for preparing nanoscale MOFs (NMOFs) using reverse microemulsions and have demonstrated their utility as magnetic resonance imaging contrast agents.[3] Owing to their tunable nature, we believe that NMOFs have potential in a variety of other imaging, biosensing, biolabeling, and drug delivery applications. The successful application of NMOFs in these areas will critically depend on our ability to modify and functionalize their surfaces to engender stability, biocompatibility, and specific functionality. To date, however, there have been no reports on the surface modification or functionalization of MOF materials.

Coating nanostructures with a silica shell via sol-gel or microemulsion-based methods has enabled the synthesis of an array of core-shell nanocomposites, such as silica-coated superparamagnetic metal oxides,[4] quantum dots,[5] gold,[6] carbon nanotubes,[7] and organic polymers.[8] The silica shell as a surface coating offers several advantages, including enhanced water dispersibility, biocompatibility, and the ability to further functionalize the core-shell nanostructures via the co-condensation of siloxy-derived molecules. Herein, we describe a general method for synthesizing a new class of nanocomposites with an NMOF core and a silica shell. We also demonstrate the ability to control the release of metal constituents from silica-coated NMOFs and to further functionalize them for the luminescence sensing of dipicolinic acid (DPA), which is a major constituent of many pathogenic spore-forming bacteria.

NMOFs of the composition $Ln(BDC)_{1.5}(H_2O)_2$, **1**, where $Ln=Eu^{3+}$, Gd^{3+}, or Tb^{3+} and BDC=1,4-benzenedicarboxylate, were synthesized using a reverse microemulsion system as previously described (**1′** is used to designate Eu-doped $Gd(BDC)_{1.5}(H_2O)_2$ in Scheme 1).[3] This synthesis allowed for the aspect ratios of nanorods **1** to be reproducibly tuned from 2.5 to 40 by adjusting the water to surfactant molar ratio, *W*. We then used a strategy developed by van Blaaderen et al. to deposit silica on NMOFs whose surfaces had been modified with polyvinylpyrrolidone (PVP).[9] Treatment of as-synthesized **1** with PVP (MW=40000) *in situ* for 12 h led to highly dispersible PVP-coated nanorods.

TEM showed that PVP-functionalized $Ln(BDC)_{1.5}(H_2O)_2$ nanoparticles, **2**, synthesized at *W*=5 had a rod-like morphology with dimensions approximately 100 nm in length by 40 nm in width (Figure 1b). The polydispersity of nanoparticles of **2** was low and their particle size

wlin@unc.edu.

Supporting Information Available: Experimental procedures and 17 figures. This material is available free of charge via the Internet at http://pubs.acs.org.

and morphology corresponded well to those of **1**.[3] Nanoparticles of **2** with an aspect ratio as high as 40 were also synthesized in high yield at *W*=15.

Nanoparticles of **2** were subsequently coated with silica shells of variable thickness using a sol-gel procedure. **2** was first primed with silica by treating with tetraethyl orthosilicate (TEOS, 5 μL per mg of **2** synthesized at *W*<10) in a solution of 4% (v/v) aqueous ammonia in ethanol (~0.2 mg of **2**/mL) for 2 h. An additional aliquot of TEOS (5 μL per mg of **2**) was then added and the mixture was stirred for a period of time (up to 7 h) to afford a silica shell of desired thickness. For example, an uneven silica shell of 2−3 nm in thickness was deposited on the surface of **2** after 3 h (Figure 1c), whereas a silica shell thickness of 8−9 nm was achieved simply by prolonging the reaction time to 7 h (Figure 1d). For **2** with high aspect ratios (*W*>10), the reaction conditions were slightly modified to minimize the formation of secondary silica nuclei (Supporting Information). Representative TEM images for **3** synthesized at *W*=15 with thin (2−3 nm) and thick (8−9 nm) silica coatings are shown in Figure 1e-g.

The compositions of **2** and **3** were further established by TGA (Figures 2a-b) and powder X-ray diffraction (PXRD). TGA results showed that **2** had a slight increase of the total weight loss over that of **1** as a result of the PVP coating (5.5% for *W*=5 and 1.5% for *W*=15). In contrast, the weight loss for **3** decreased significantly due to the presence of a SiO_2 coating. For **3** synthesized at *W*=5, a 2−3 nm silica coating led to a 9.6% reduction in weight loss, whereas an 8−9 nm coating of silica reduced the total weight loss by 28.5%. For **3** synthesized at *W*=15, a 2−3 nm silica coating led to a 9.4% reduction in weight loss, whereas an 8−9 nm coating of silica reduced the total weight loss by 25.7%. The smaller changes to total weight loss for **2** and **3** synthesized at *W*=15 were consistent with the reduced surface areas for larger particles. PXRD studies showed that **2** and **3** exhibited the same pattern as macroscopic **1,** further proving the presence of the crystalline NMOF core in both PVP- and silica-coated **1**. Interestingly, the NMOF core of **3** could be completely removed (via dissolution) at low pH to afford hollow silica shells with varied thickness and aspect ratios (Figure 1h). Since the morphologies of NMOFs can be controlled by exploiting the energetics of different crystallographic faces, we believe the present approach can be used to produce interesting nanoshells that are not accessible with presently available templates.

We have also examined the stabilizing effect of an 8−9 nm silica shell on the NMOF core. Figure 2c shows the dissolution curves for **1** and **3** when dialyzed against water at 37 °C. The dissolution curves for both **1** and **3** at pH=4 can be modeled as a zeroth order rate law with an apparent rate constant of 0.143 and 0.084 μM/h, respectively. The silica shell of **3** has thus stabilized the NMOF core against dissolution. A similar stabilizing effect of the silica shell was also observed at pH=5, with an apparent rate constant of 0.085 and 0.044 μM/h for **1** and **3**, respectively. These results indicate that the rates of cargo release from such core-shell nanostructures can be readily controlled, presumably by taking advantage of slow diffusion of metal and organic constituents through the silica shell.

To illustrate the utility of NMOF-based core-shell nanostructures, we have prepared Eu-doped $Gd(BDC)_{1.5}$-$(H_2O)_2$@SiO_2 nanoparticles (**3′**) at *W*=5 and further functionalized the silica surface with a silylated Tb-EDTA monoamide derivative, **3′**-Tb-EDTM (Scheme 1). Tb^{3+}-ions[10] and molecular Tb complexes [11] have been used as sensitive luminescence probes for Anthrax and other bacterial spores by complexing to DPA, which constitutes up to 15% of the spores' dry mass. Upon excitation at 278 nm, **3′**-Tb-EDTM only gave Eu luminescence because the Tb-EDTM moiety is essentially non-emissive. As DPA was added to an ethanolic dispersion of **3′**-Tb-EDTM, the Tb luminescence became clearly visible due to the formation of the Tb-EDTM-DPA complex. The Tb luminescence signal provides a sensitive probe for DPA detection while the Eu emission from the NMOF core acts as non-interfering internal calibration. As shown in Figure 2d, the relationship between the ratio of Tb to Eu emission

intensities and DPA concentration displayed normal saturation behavior. At low DPA concentrations, the ratio of signal intensities increased linearly; however, the ratio of intensities began to level off as the Tb-EDTA complexes became coordinatively saturated with DPA. The DPA detection limit for this system was estimated to be ~48 nM. Such a ratiomeric sensing scheme works equally well in a Tris buffer solution and is able to selectively detect DPA in the presence of biologically prevalent interferences such as amino acids (Supporting Information).

In summary, we have developed a general method to coat NMOFs with silica shells of variable thickness. These shells increase NMOF core stability and allow for the controlled release of metal constituents. Silica-coated NMOFs were further functionalized for the detection of DPA, an important molecular marker in spore-producing bacteria. Owing to the tunability of NMOF composition and morphology, the present approach should allow for the synthesis of novel core-shell hybrid nanostructures for future imaging, sensing, and drug delivery applications.

Supplementary Material

Refer to Web version on PubMed Central for supplementary material.

Acknowledgement

We acknowledge financial support from NSF and NIH grants. WJR thanks NSF for a graduate research fellowship and WL is a Camille Dreyfus Teacher-Scholar.

References

1. a Wu H, Zhou W, Yildirim T. J. Am. Chem. Soc 2007;129:5314. [PubMed: 17425313] b Kesanli B, Cui Y, Smith M, Bittner E, Bockrath B, Lin W. Angew. Chem., Int. Ed 2005;44:72. c Rowsell JLC, Yaghi OM. Angew. Chem. Int. Ed 2005;44:4670.
2. a Wu C, Hu A, Zhang L, Lin W. J. Am. Chem. Soc 2005;127:8940. [PubMed: 15969557] b Cho SH, Ma B, Nguyen ST, Hupp JT, Albrecht-Schmitt TE. Chem. Commun 2006:2563. c Wu C-D, Lin W. Angew. Chem. Int. Ed 2007;46:1075.
3. Rieter WJ, Taylor KML, An HY, Lin W, Lin W. J. Am. Chem. Soc 2006;128:9024. [PubMed: 16834362]
4. a Lu Y, Yin Y, Mayers BT, Xia Y. Nano Lett 2002;2:183. b Yi DK, Selvan ST, Lee SS, Papaefthymiou GC, Kundaliya D, Ying JY. J. Am. Chem. Soc 2005;127:4990. [PubMed: 15810812]
5. a Selvan ST, Patra PK, Ang CY, Ying JY. Angew. Chem. Int. Ed 2007;46:2448. b Selvan ST, Tan TT, Ying JY. Adv. Mater 2005;17:1620.
6. LizMarzan LM, Giersig M, Mulvaney P. Langmuir 1996;12:4329.
7. Fu Q, Lu C, Liu J. Nano Lett 2002;2:329.
8. a Deng ZW, Chen M, Zhou SX, You B, Wu LM. Langmuir 2006;22:6403. [PubMed: 16800706] b Jiang P, Bertone JF, Colvin VL. Science 2001;291:453. [PubMed: 11161193] c Caruso F, Caruso RA, Mohwald H. Science 1998;282:1111. [PubMed: 9804547]
9. Graf C, Vossen DLJ, Imhof A, van Blaaderen A. Langmuir 2003;19:6693.
10. a Rosen DL, Sharpless C, McGown LB. Anal. Chem 1997;69:1082. b Pellegrino PM, Fell NF Jr. Rosen DL, Gillespie JB. Anal. Chem 1998;70:1755. c Hindle AA, Hall EAH. Analyst 1999;124:1599. [PubMed: 10746319]
11. Cable ML, Kirby JP, Sorasaenee K, Gray HB, Ponce A. J. Am. Chem. Soc 2007;129:1474. [PubMed: 17243674]

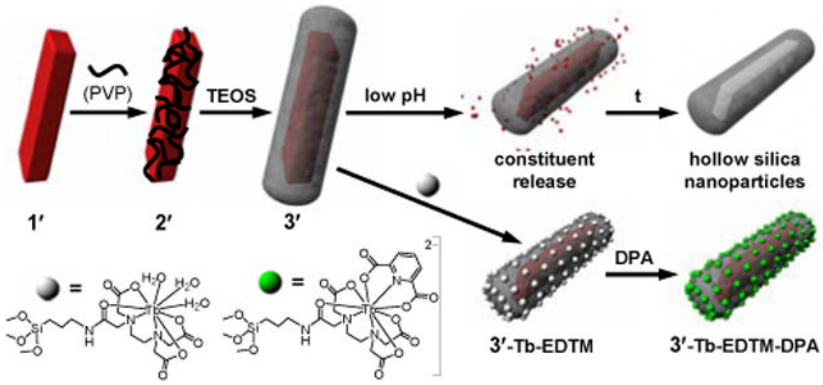

Scheme 1.

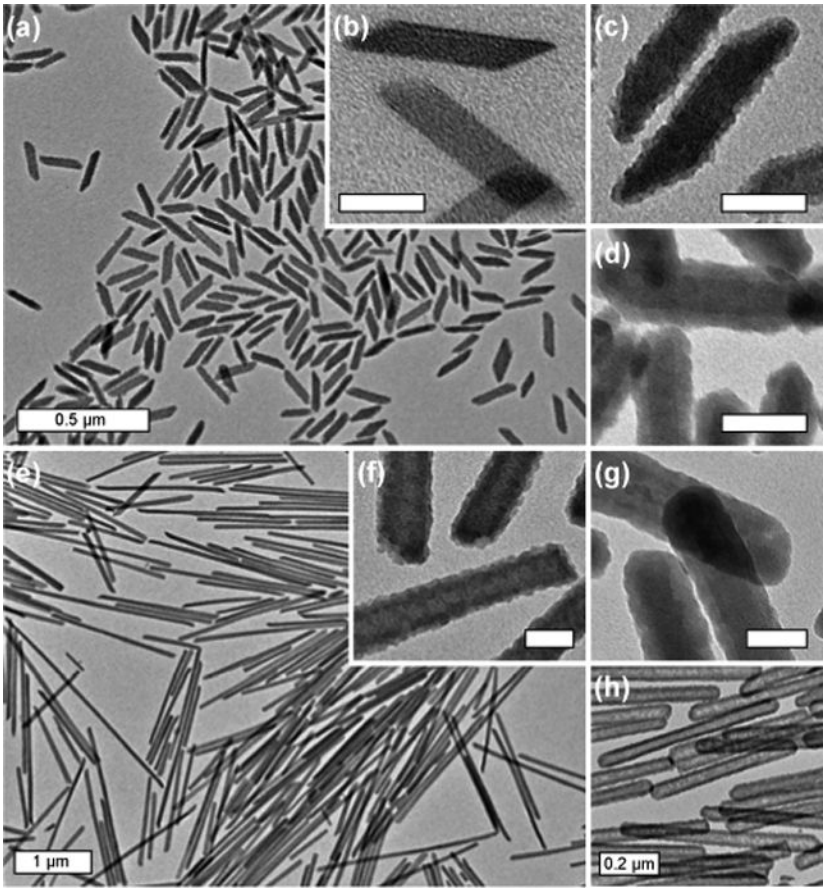

Figure 1.
(a and c) TEM images of **3** with a 2−3 nm silica shell (*W*=5); (b) TEM image of **2** (*W*=5); (d) TEM image of **3** with an 8−9 nm silica shell (*W*=5); (e and f) TEM images of **3** with a 2−3 nm silica shell (*W*=15); (g) TEM image of **3** with an 8−9 nm silica shell (*W*=15); (h) TEM image of 8−9 nm silica nanoshells generated from (g). Scale bars are 50 nm unless otherwise indicated.

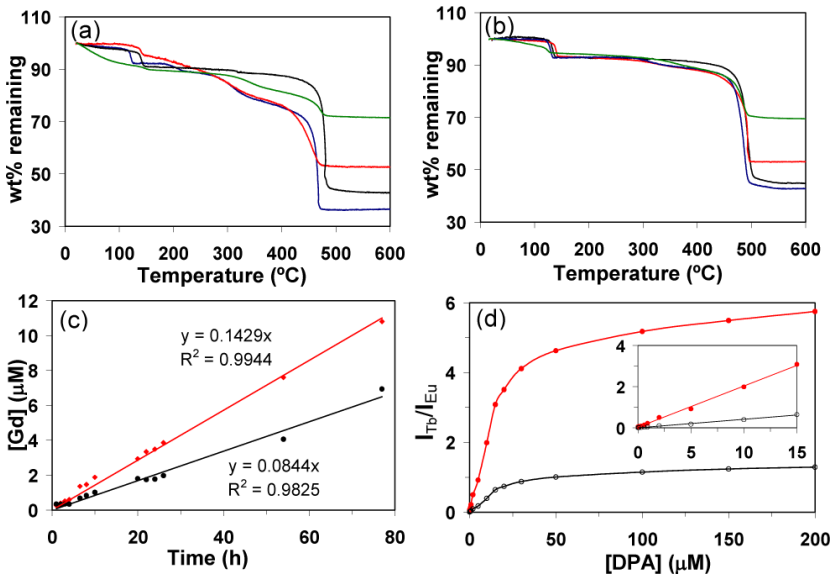

Figure 2.

TGA curves for **1**−**3** synthesized at (a) *W*=5 and at (b) *W*=15 (black=**1**; blue=**2**; red=**3** with a 2−3 nm silica shell; green=**3** with an 8−9 nm silica shell). (c) Time-dependent dissolution curves for **1** (red) and **3** (black) with an 8−9 nm silica shell at pH=4 and 37 °C. (d) Dependence of the ratio of Tb to Eu emission intensities for **3′**-Tb-EDTM on DPA concentration (red=544 nm/592 nm, black=544 nm/615 nm). The inset shows the linear relationship at low [DPA].